Electronic Supplementary Material (ESI) for Nanoscale.

Supramolecular Alternate Donor–Acceptor Copolymers Mediated by Pt···Pt Metal–Metal Interactions and Their Photocatalytic Applications

*Zhao Gao, Zijian Li, Zongchun Gao, and Feng Wang**

CAS Key Laboratory of Soft Matter Chemistry,
iChEM (Collaborative Innovation Center of Chemistry for Energy Materials),
Department of Polymer Science and Engineering,
University of Science and Technology of China,
Hefei, 230026, China
Fax: (+86) 551 6360 6095; E-mail: drfwang@ustc.edu.cn.

Supporting Information

1. Materials and methods

Copper iodide (CuI), 4-dimethylamino pyridine (DMAP), *N*-(3-(dimethylamino)propyl)-*N*'-ethylcarbodiimide hydrochloride (EDC•HCl), and benzyltriethylammonium chloride (TEBAC) were reagent grade and used as received. Compound **3a**, **3b**, **4**, **6** and **9** were synthesized according to the previously reported procedures.[S1–S5] Other reagents and solvents were employed as purchased.

^{1}H NMR spectra were collected on a Varian Unity INOVA-300 spectrometer with TMS as the internal standard. ^{13}C NMR spectra were recorded on a Varian Unity INOVA-300 spectrometer at 75 MHz. MALDI-TOF measurements were recorded on a Bruker Autoflex Speed spectrometer with DCTB as the matrix. UV–Vis spectra were recorded on a UV-1800 Shimadzu spectrometer. Solution excitation and steady-state fluorescence emission spectra were recorded on a FluoroMax-4 spectrofluorometer (Horiba Scientific) and analyzed with an Origin (v8.0) integrated software FluoroEssence (v2.2). Electron spin resonance (ESR) measurements were performed on a JEOL JES-FA200 apparatus, with the utilization of 2,2,6,6-tetra-methylpiperidine as the spin trap for $^{1}O_2$. Dynamic light scattering (DLS) experiments were conducted on a Malvern Zeta-sizer Nano ZS Instrument. Transmission electron microscope (TEM) images were performed on a Tecnai G2 Spirit BioTWIN electron microscope (acceleration voltage: 120 kV).

2. *Mathematical models to fit the spectroscopic melting curves*

2.1 Mathematical model for cooperative assembling process

In terms of **1a**, it adopts cooperative mechanism for the supramolecular assembling process. To acquire the detailed thermodynamic parameters for the self-assembly process, Meijer–Schenning–Van-der-Schoot model has been employed to fit the melting curves.[S6] In detail, a non-sigmoidal curve can be obtained by plotting the fraction of aggregated species (α_{agg}) against temperature at 500 nm on the basis of temperature-dependent UV–Vis absorption spectra experiments. The supramolecular polymerization can be divided into two separated steps: the nucleation and elongation regimes. In the elongation regime, the fraction of aggregated molecules φ_n is described by Eq. S1:

$$\varphi_n = \varphi_{SAT}\{1 - exp[(-h_e) \times (T - T_e)/(R \times T_e^2)]\} \quad \text{(Eq. S1)}$$

In this equation, h_e denotes the molecular enthalpy release due to the non-covalent supramolecular polymerization, T and T_e stand for the absolute temperature and elongation temperature, respectively. R represents the universal gas constant. φ_{SAT} is a parameter that is introduced to prevent the relation φ_n/φ_{SAT} surpassing the value of one.

In the nucleation regime, it means that at temperatures below the elongation temperature T_e. φ_n is described by Eq. S2:

$$\varphi_n = {K_a}^{1/3} \times exp\left[\left(2/3K_a^{-1/3} - 1\right) \times h_e \times (T - T_e)/(R \times {T_e}^2)\right] \quad \text{(Eq. S2)}$$

K_a is the dimensionless equilibrium constant for the nucleation step at T_e. It is apparent that the data points are accurately fitted over the whole temperature range. The detailed thermodynamic parameters are shown in Table S1 (*vide infra*).

2.2 Mathematical model for isodesmic assembling process

For the isodesmic model[S7] adopted by complex **1a/2**, the obtained fraction of aggregates (α) versus temperature (T) was fitted according to Eq. S3:

$$\alpha\left(T\right) = \frac{1}{1 + \exp\left[\frac{T - T_m}{T^*}\right]} \quad \text{(Eq. S3)}$$

T_m is the temperature at which α is 0.5.

The number averaged degree polymerization (DP_N) at various temperatures was calculated using Eq. S4:

$$DP_N(T) = \frac{1}{\sqrt{1 - \alpha(T)}} \quad \text{(Eq. S4)}$$

3. *Self-assembly of **1a***

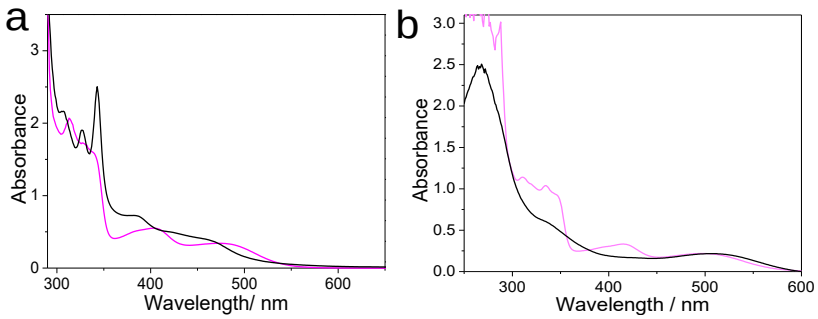

Figure S1. UV–Vis absorption spectra of a) **1a**, and b) **1b** in DCE (pink line) and MCH/DCE (95 : 5, *v*/*v*) (black line). For **1a**, the maximum MLCT/LLCT absorption band at molecularly dissolved state is located at 483 nm. Upon varying the solvent from pure DCE to apolar MCH/DCE (95 : 5, *v*/*v*), the MLCT/LLCT absorption displays a hypochromic shift (λ_{max} = 467 nm), suggesting the aggregation of platinum(II) terpyridine moiety. For **1b** in MCH/DCE (95 : 5, *v*/*v*), a shoulder band between 510 and 580 nm emerged, which is assigned to the MMLCT band absorption. No MMLCT band can be observed in UV–Vis spectrum of **1a**. Such phenomena validate the feasibility to rule out Pt(II)···Pt(II) interactions during the **1a** self-assembly process, by attaching three bulky *tert*-butyl units.

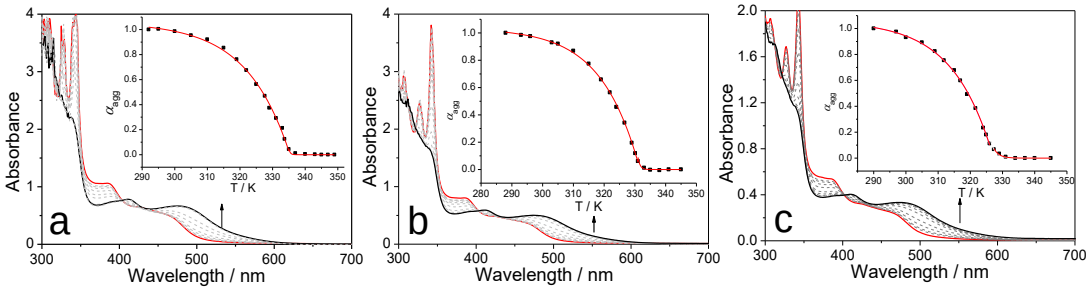

Figure S2. Temperature-dependent UV–Vis absorption spectra of **1a**, a) 0.20 mM; b) 0.15 mM; c) 0.10 mM in MCH/DCE (95 : 5, *v*/*v*). Arrows indicate the spectral changes upon increasing temperature. Inset: α_{agg} as a function of temperature for **1a** (λ = 500 nm). Non-linear fitting of the normalized curve with the Meijer–Schenning–Van-der-Schoot mathematical model affords the corresponding thermodynamic parameters (Table S1).

Table S1. Thermodynamic parameters of **1a** in MCH/DCE (95 : 5, *v*/*v*) obtained by fitting the temperature-dependent UV–Vis absorption data.

Concentration [mM]	T_e [K]	h_e [kJ mol^{-1}]
0.20	335.4	–70.9
0.15	331.6	–73.5
0.10	327.2	–71.5

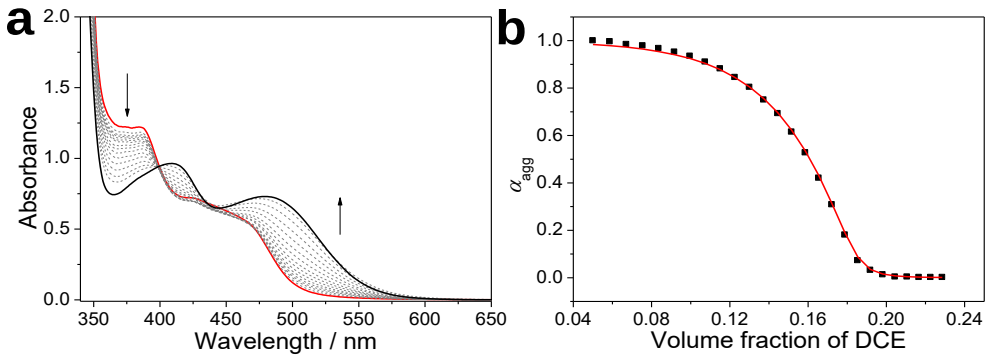

Figure S3. a) Solvent-dependent UV–Vis absorption spectra of **1a** (0.20 mM in MCH/DCE). Arrows indicate the spectral changes upon increasing the DCE content. b) Plot of normalized degree of aggregation *versus* volume fraction of DCE monitored at λ = 500 nm. It affords a non-sigmoidal curve, suggesting the involvement of cooperative nucleation–elongation mechanism for the **1a** self-assembly process. Depending on the non-linear fitting of the normalized curve with the solvent-dependent mathematical model,[S8] $\Delta G°'_{(f=0.05)}$ (Gibbs free energy gain upon monomer addition) and σ (cooperavity parameter) are determined to be –26.3 kJ mol^{-1} and 0.001, respectively.

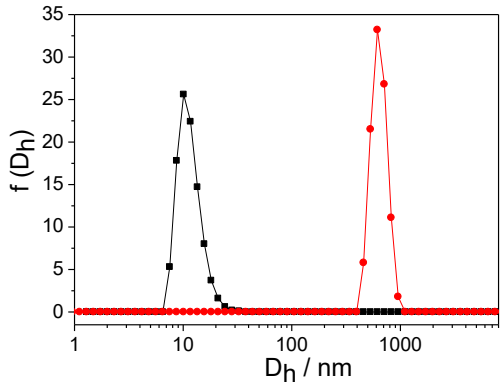

Figure S4. DLS measurement of **1a** (0.10 mM) in DCE (black line) and MCH/DCE (95 : 5, *v*/*v*) (red line). When switching the solvent from DCE to MCH/DCE (95 : 5, *v*/*v*), the averaged hydrodynamic radius increases from 10 nm (molecular dissolved state) to 615 nm.

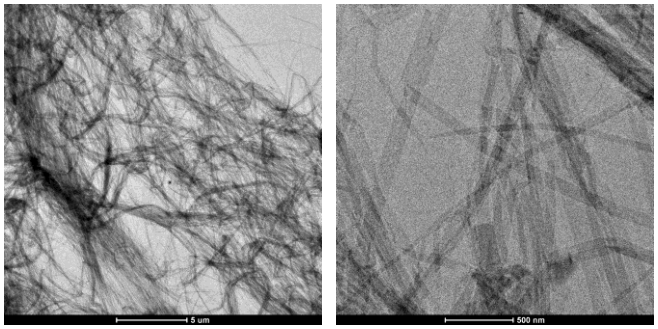

Figure S5. TEM micrograph obtained by dropping **1a** [MCH/DCE (95 : 5, *v*/*v*), 0.40 mM] on a copper grid.

4. Self-assembly of ***2***

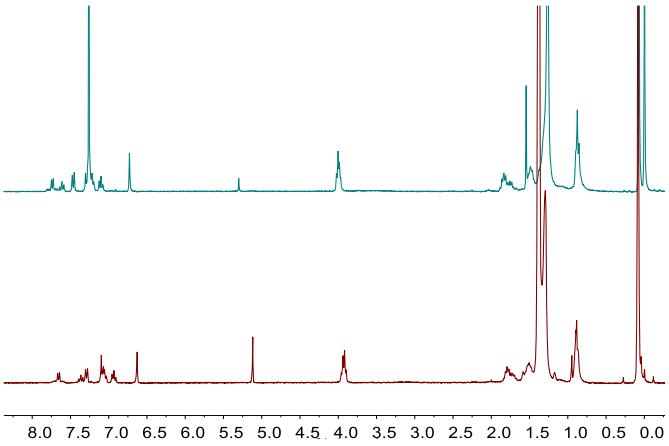

Figure S6. ^{1}H NMR spectrum (300 MHz, room temperature) of **2** (2.00 mM) in $CDCl_3$ (top) and *d*-cyclohexane/$CDCl_3$ (95 : 5, *v*/*v*) (down). ^{1}H NMR resonances hardly shift upon varying the solvent polarity, indicating the absence of close π–π and Pt(II)···Pt(II) interactions for the platinum(II) diphenylpyridine units on **2**.

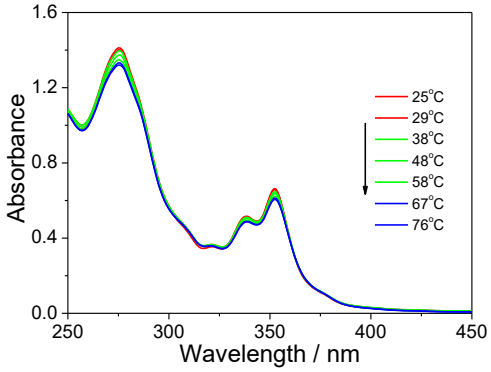

Figure S7. Temperature-dependent UV–Vis absorption spectra of **2** (0.10 mM) in MCH/DCE (95 : 5, *v*/*v*). Only a small decrease of the absorbance intensity can be observed upon increasing the temperature.

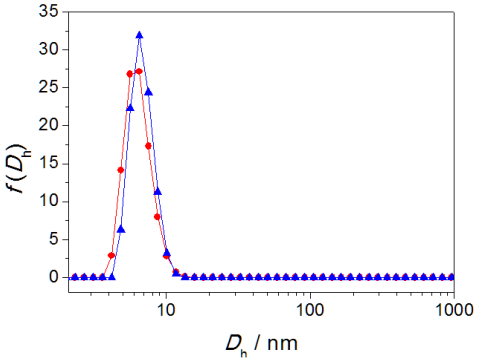

Figure S8. DLS measurement of **2** (0.10 mM) in DCE (red) and MCH/DCE (95 : 5, *v*/*v*) (blue). The hydrodynamic diameters from DCE (6.0 nm) to MCH/DCE (95 : 5, *v*/*v*) (6.5 nm) shows minor changes. Hence, **2** exhibits rather weak self-aggregation tendency in the latter solvent.

*5. Spectroscopic and morphological measurements of complex **1a/2***

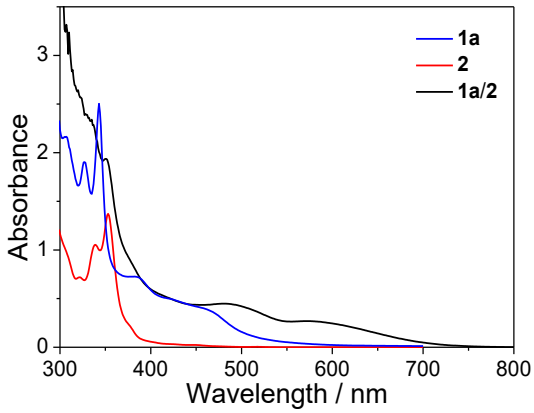

Figure S9. UV−Vis spectra of **1a**, **2** and **1a/2** in MCH/DCE (95 : 5, *v*/*v*, 0.10 mM for each monomer).

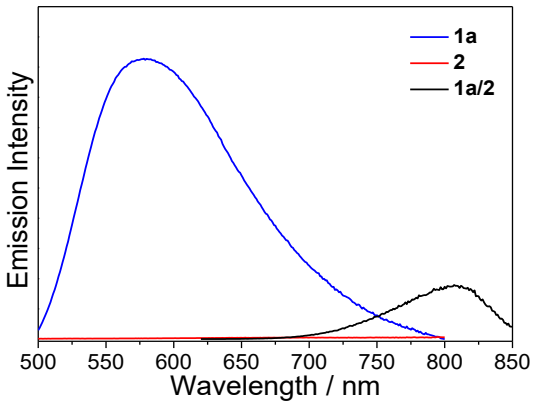

Figure S10. Fluorescent spectra of **1a**, **2**, and **1a**/**2** in MCH/DCE (95 : 5, *v*/*v*, 0.10 mM for each monomer). Complex **1a**/**2** shows a near-infrared emission band centered at 810 nm, which has relatively lower energy than the MLCT/LLCT emission band of **1a** (λ_{max} = 580 nm). This emission band can be typically assigned to the MMLCT transition, demonstrating the involvement of intermolecular Pt(II)···Pt(II) interactions for complex **1a**/**2**.

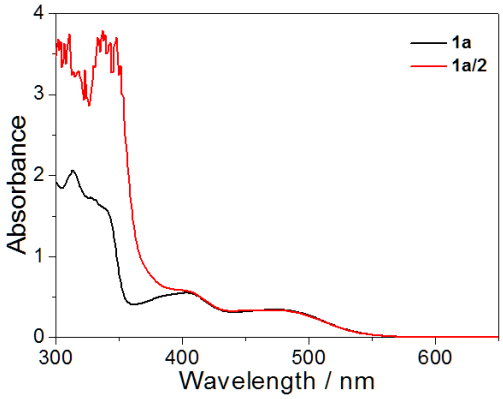

Figure S11. UV–Vis absorption spectra of **1a** and **1a**/**2** in DCE, respectively. Upon mixing **1a** and **2** together in DCE, it shows the overlap of the absorbance from the individual species.

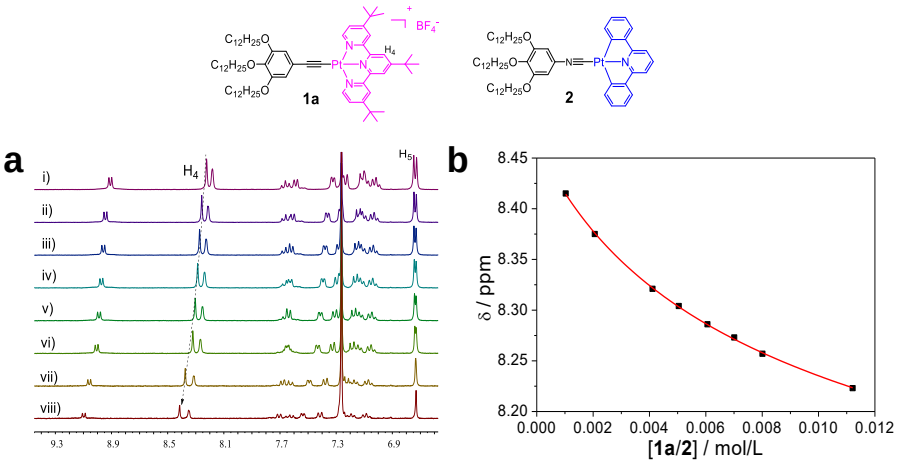

Figure S12. a) Partial ^{1}H NMR spectra (300 MHz, $CDCl_3$, 298 K) of a 1 : 1 mixture of **1a** and **2** at different monomer concentrations (from 11.0 mM of *i* to 1.00 mM of *viii*). b) Chemical resonances change for protons H_4 on **1a** and the nonlinear curve fittings.[S9] Upon dilution, the pincer ^{1}H NMR protons on **1a** and **2** (the terpyridine and diphenylpyridine siganls, respectively) shift downfield. The association constant (K_a) value is determined to be 51 ± 3.5 M^{-1} in *d*-chloroform, by treating the collected chemical shift changes of proton H_4 with a nonlinear curve-fitting equation.

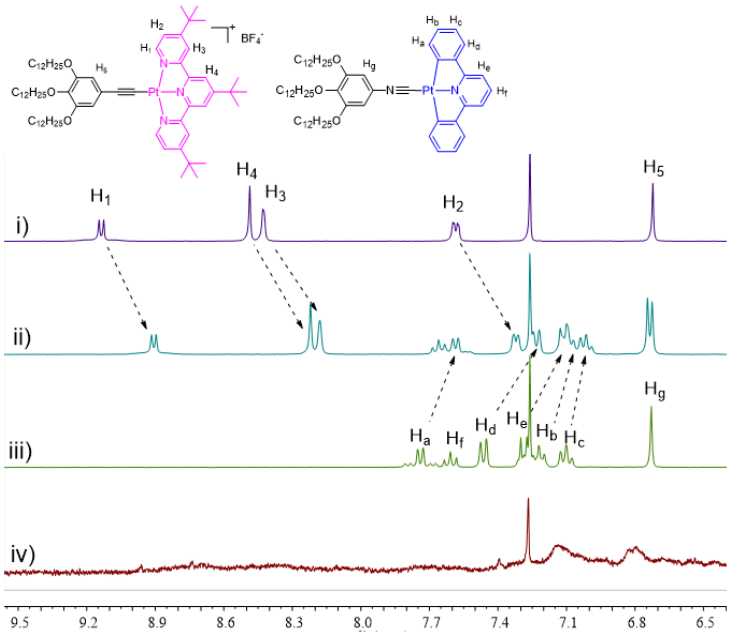

Figure S13. Partial ^{1}H NMR spectra (300 MHz, 298 K, 2.00 mM) of i) **1a**, ii) **1a**/**2**, and iii) **2** in $CDCl_3$, and iv) **1a**/**2** in d_{12}-cyclohexane. As compared to the individual species, upfield ^{1}H NMR resonances can be observed for an equimolar mixture of **1a** and **2** ($\Delta\delta$ = 0.23, 0.27, 0.25, 0.27 for $H_{1–4}$ on **1**, and 0.15, 0.13, 0.09, 0.23, 0.17 ppm for $H_{a–e}$ on **2**, respectively) in $CDCl_3$. In apolar d_{12}-cyclohexane, the ^{1}H NMR aromatic protons become broad and indistinguishable from the baseline noise. Hence, it suggests the presence of complementary donor–acceptor interactions between **1a** and **2**.

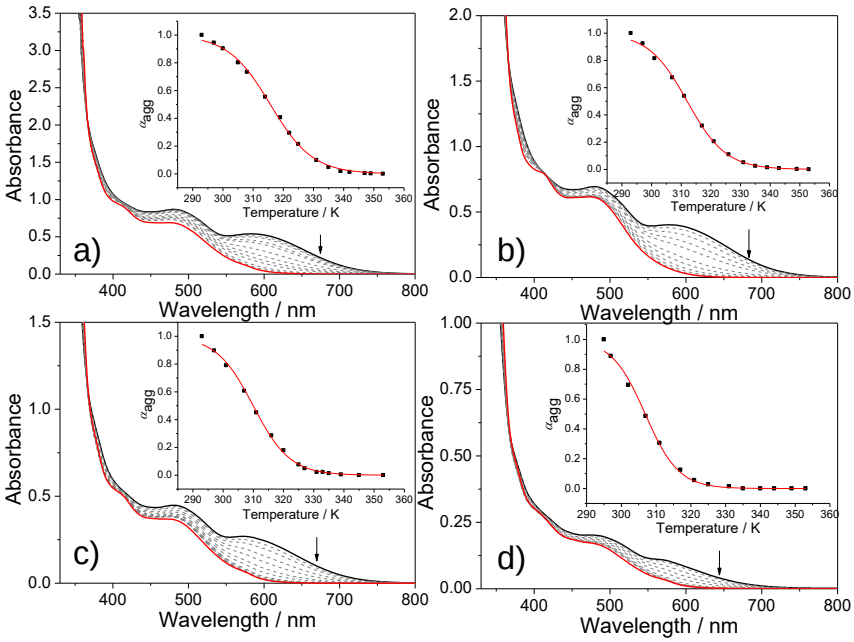

Figure S14. Temperature-dependent UV–Vis absorption spectra of **1a**/**2**: a) 0.25 mM; b) 0.15 mM; c) 0.10 mM; d) 0.05 mM in MCH/DCE (95 : 5, *v*/*v*). Inset: α_{agg} as a function of temperature. The normalized melting curves at λ = 600 nm display sigmoidal curves, which are characteristic for the isodesmic assembling mechanism. Non-linear fitting of the normalized curve with Eq. S3 affords the corresponding thermodynamic parameters.

Table S2. Thermodynamic parameters of co-assembly **1a/2** in MCH/DCE (95 : 5, *v*/*v*), which are obtained by fitting the temperature-dependent UV–Vis data.

Concentration [mM]	Melting temperature T_m [K]	Enthalpy of polymerization ΔH [kJ mol^{-1}]	DP_N*
0.25	315.7	–149.1	5.13
0.15	312.0	–152.0	4.42
0.10	310.0	–147.4	4.14
0.05	306.9	–170.0	4.02

* Temperature at 293 K.

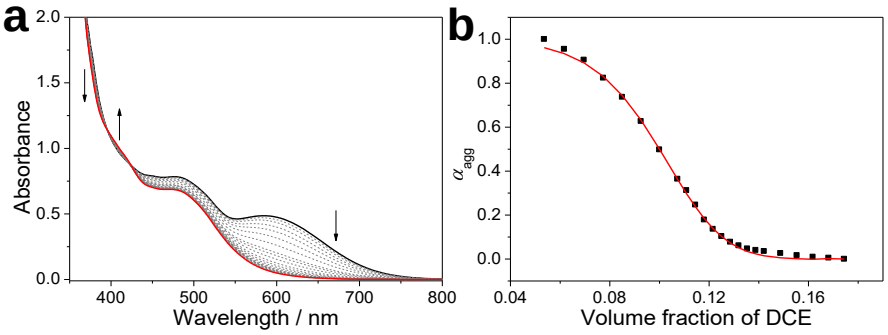

Figure S15. a) Solvent-dependent UV–Vis absorption spectra of **1a/2** (0.20 mM in

MCH/DCE). Arrows indicate the spectral changes upon increasing DCE content. b) Plot of normalized degree of aggregation *versus* volume fraction of DCE monitored at λ = 600 nm. The sigmoidal curve indicates an isodesmic co-assembly mechanism for **1a**/**2** complex in apolar MCH/DCE medium. Depending on the non-linear fitting of the normalized curve with the solvent-dependent mathematical model,[S8] $\Delta G^{\circ}{}'_{(f=0.05)}$ (Gibbs free energy gain upon monomer addition) and σ (cooperavity parameter) are determined to be –27.9 kJ mol^{-1} and 1, respectively.

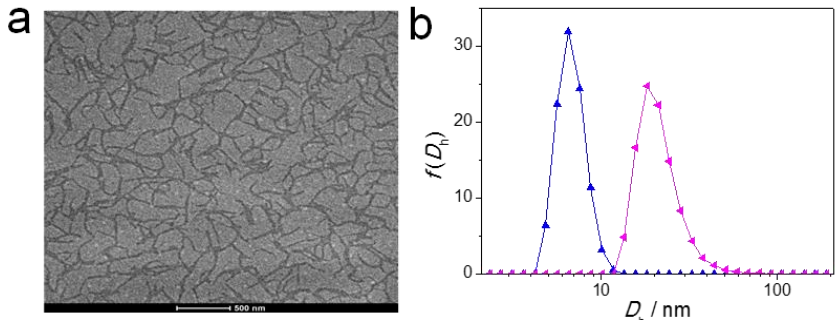

Figure S16. a) TEM micrograph obtained by dropping of **1a**/**2** in MCH/DCE (95 : 5, *v*/*v*, 0.40 mM) on a copper grid. b) DLS measurement of **1a**/**2** (0.10 mM) in DCE (blue) and MCH/DCE (95 : 5, *v*/*v*) (pink).

*6. Determination of D–A arrangement for **1a/2***

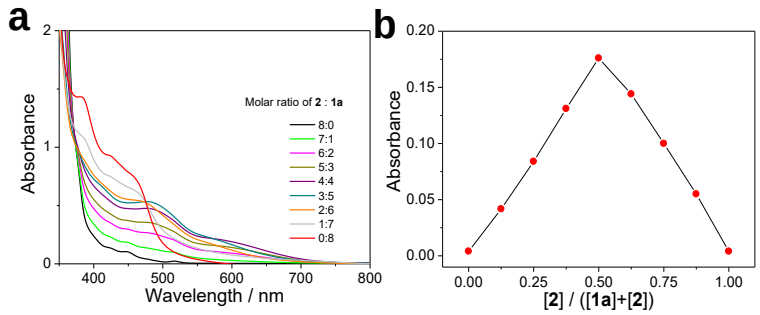

Figure S17. Job's plot between **1a** and **2** (MCH/DCE (95 : 5, *v*/*v*)), by plotting the intensity changes of UV–Vis MMLCT absorbance band at 610 nm against the mole fraction of **2**. When the amounts of **1a** and **2** are equivalent to each other, the MMLCT absorption intensity reaches to the maximum value, suggesting the 1 : 1 binding stoichiometry between **1a** and **2**.

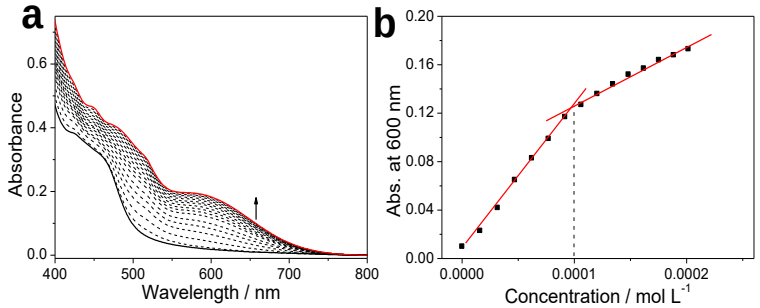

Figure S18. UV–Vis absorption spectra change upon gradual addition of **2** into **1a** (MCH/DCE (95 : 5, *v*/*v*)). The resulting molar ratio plot suggests 1 : 1 binding stoichiometry between **2** and **1a**, which is consistent with the Job's plot results (Fig. S14).

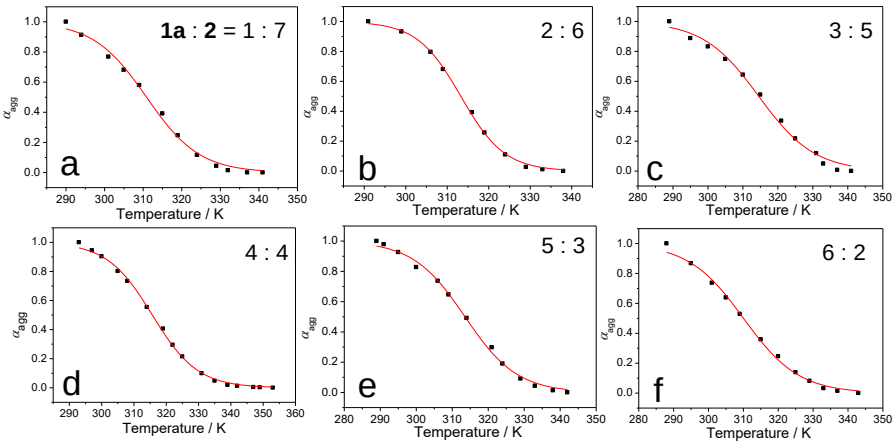

Figure S19. Monitoring the UV–Vis MMLCT absorbance band at 600 nm (MCH/DCE (95 : 5, *v*/*v*)) *versus* temperature at different molar ratio of **1a** : **2**: a) 1 : 7, b) 2 : 6, c) 3 : 5, d) 4 : 4, e) 5 : 3, and f) 6 : 2. T_m values were plotted *versus* the molar ratio of **1a** and **2**, while keeping the total concentration constant (0.50 mM). The maximum T_m (315.7 K) was attained when the molar ratio of **1a**/**2** reaches to 1 : 1 (see Fig 2a in the main text), which unambiguously support the formation of alternated arrangement between **1a** and **2**.

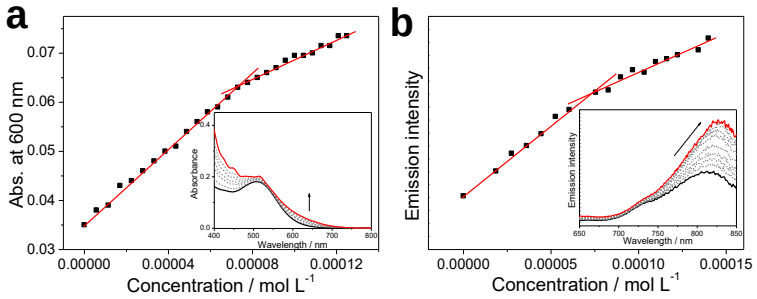

Figure S20. a) UV–Vis absorption, and b) fluorescent spectra change upon gradual addition of **2** into **1b** (MCH/DCE (95 : 5, *v*/*v*)). Upon progressive titrating **2** (1.00 mM) into **1b** (0.10 mM), MMLCT spectroscopic signals display slight increase for their intensities. Depending on both UV–Vis and fluorescent titration experiments, the molar ratio plots suggest non-equivalent complexatation stoichiometry between **2** and **1b** (the inflection points are around 0.7 for [**2**]/[**1b**]). Hence, complex **1b/2** prefers to adopt randomly mixing arrangement.

*7. Visible-light photosensitization capability of **1a/2***

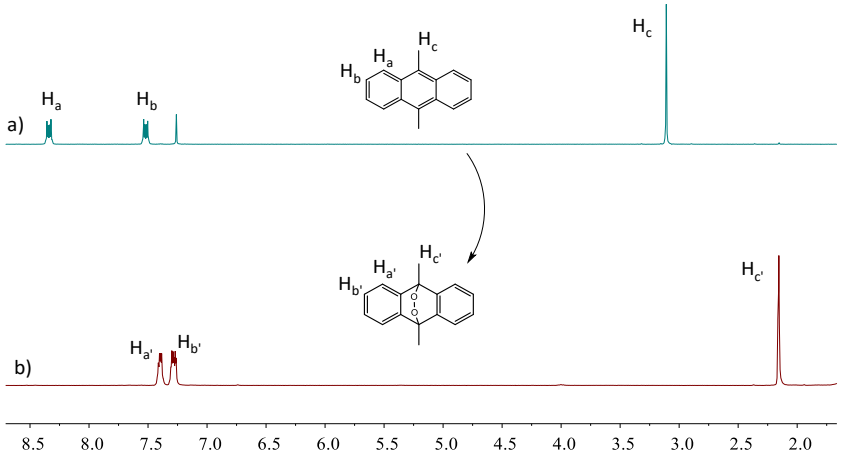

Figure S21. Partial ^{1}H NMR spectrum (300 MHz, room temperature) of 9,10-dimethylanthracene (DMA) (20.0 mM) and **1a/2** (0.20 mM): a) before, and b) after 12 hours visible light irradiation (590 nm, 12 W). The formation of 9,10-dimethylanthracene-9,10-endoperoxide from DMA by 590 nm irradiating can be directly proved by ^{1}H NMR spectra, which indicates the capture of DMA by $^1O_2$ at the presence of catalytic equivalent **1a/2**.

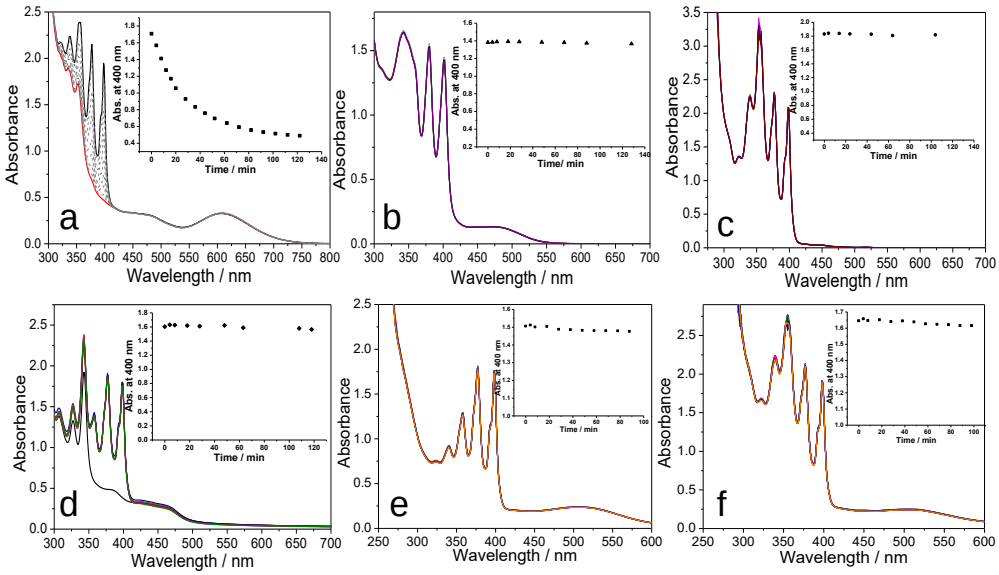

Figure S22. UV–Vis absorption spectra of DMA with catalytic equivalent of **1a**/**2** in a) MCH/DCE (95 : 5, *v*/*v*), b) DCE, and c) **2**, d) **1a**, e) **1b**, f) **1b/2** in MCH/DCE (95 : 5, *v*/*v*) upon irradiating at 590 nm. Inset: the collected absorbance data at 400 nm *versus* irradiation time.

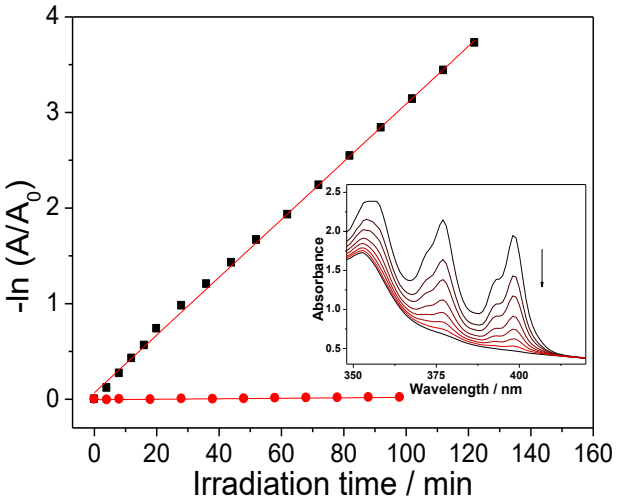

Figure S23. Plots of –ln(A/A_0) *versus* irradiation time for the photooxidation of DMA (data collected from the UV–Vis absorption changes at 400 nm). Inset: UV–Vis absorption intensities of DMA with catalytic equivalent photocatalyst gradually decrease upon irradiating at the visible-light region. Complex **1b**/**2** displays rather weak $^1O_2$ generation capability, as evidenced by the significantly lower rate constant than that of **1a**/**2** (2.48×10^{-4} min^{-1} *versus* 3.02×10^{-2} min^{-1}).

*8. Visible-light photocatalytic behaviors of **1a/2***

General procedure for the photocatalytic reaction: photo-oxidation reaction of *α*-terpinene was investigated with a 13 cm-tall quartz tube (10 mm inner diameter). The irradiated volume of the reactor was 0.50 mL. In a distance of 5 cm to the photoreactor the light source was mounted, a LED module emitting at 590 nm with 12 W light output. The reaction mixture was bubbled with solvent-saturated oxygen gas in 30 seconds before the irradiation reactions at room temperature. Upon light irradiation, the ^{1}H NMR resonance intensity of olefinic protons of *α*-terpinene (5.63 ppm, 2H, d, J = 5.4 Hz; 5.59 ppm, 2H, d, J = 5.5 Hz) progressively decreases. In the meantime, the product ascaridole (6.50 ppm, 2H, d, J = 8.5 Hz; 6.41 ppm, 2H, d, J = 8.5 Hz) signals gradually increase (Figure S25). After irradiating for several hours, the solvent was evaporated and the conversion yield was calculated, by using 4,4'-dimethyl-2,2'-bipyridine as the internal ^{1}H NMR standard. As a comparison, **1a**, **1b**, **2**, **1b/2** were employed as the photosensitizers at the identical concentration and irradiation time.

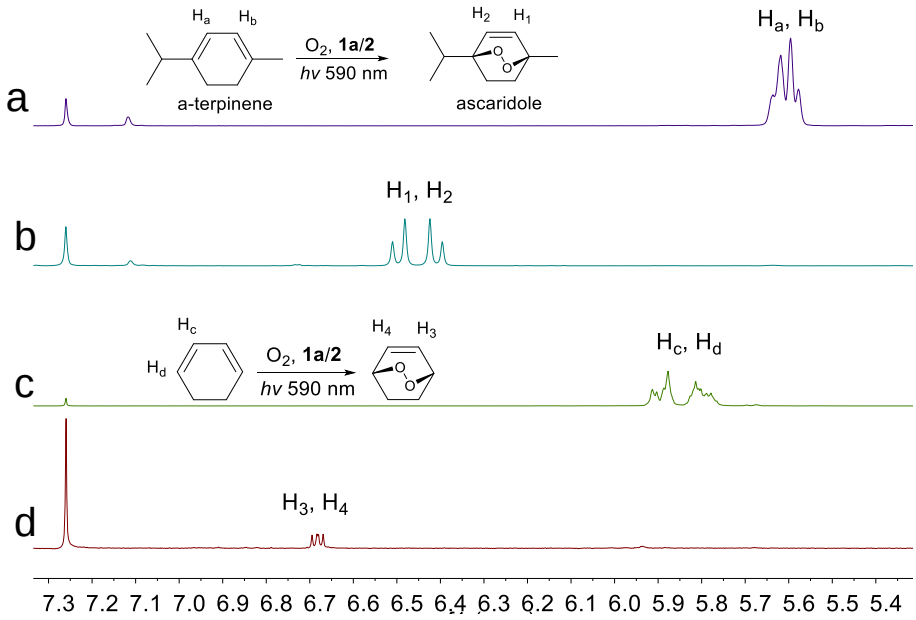

Figure S24. Partial ^{1}H NMR spectrum of a) *α*-terpinene, b) ascaridole (>99% conversion), c) 1,3-cyclohexadiene, and d) the product of 1,3-cyclohexadiene after 12 hours visible light irradiation (590 nm, 12 W).

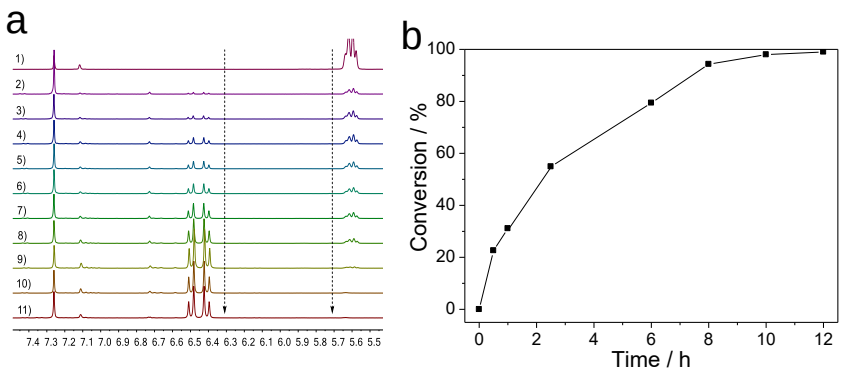

Figure S25. a) Partial ^{1}H NMR spectrum of *α*-terpinene with the increasing irradiation time. Upon visible light irradiation, the olefinic resonances of α-terpinene (5.63 ppm, 2H, d, J = 5.4 Hz; 5.59 ppm, 2H, d, J = 5.5 Hz) progressively decrease for their intensities. In the meantime, the ascaridole ^{1}H NMR signals (6.50 ppm, 2H, d, J = 8.5 Hz; 6.41 ppm, 2H, d, J = 8.5 Hz) gradually increase. b) Conversion from *α*-terpinene to ascaridole *versus* irradiation time.

We have also purified the product ascaridole from the photocatalytic reaction. In detail, after 590 nm light irradiation for 12 h, the solvent was removed with a rotary evaporator. The crude product was then purified by flash column chromatography (petroleum ether as the eluent) to afford ascaridole as a colorless liquid. The isolation yield of ascaridole is calculated to be 71%. It is highly plausible that the isolated yield is a little lower than the yield determined in ^{1}H NMR study (82%), due to the loss during the chromatography process. The products are fully characterized *via* ^{1}H, ^{13}C NMR, and ESI–MS measurements. ^{1}H NMR (300 MHz, $CDCl_3$) δ (ppm): 6.43 (d, J = 8.5 Hz, 1H), 6.34 (d, J = 8.6 Hz, 1H), 2.01–1.91 (m, 2H), 1.85 (dt, J = 13.8, 6.8 Hz, 1H), 1.45 (d, J = 10.0 Hz, 2H), 1.31 (s, 3H), 0.93 (d, J = 6.9 Hz, 6H). ^{13}C NMR (75 MHz, $CDCl_3$) δ (ppm): 135.37, 132.02, 78.77, 73.34, 31.11, 28.49, 24.58, 20.38, 16.22, 16.14. ESI–MS m/z: $[M + Na]^+$: $C_{10}H_{16}NaO_2$, 191.07.

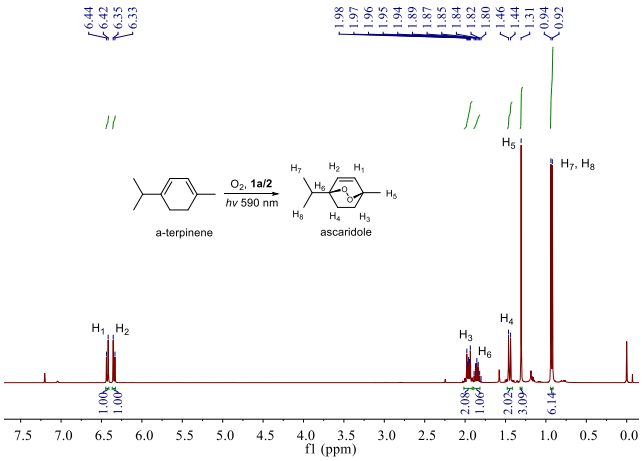

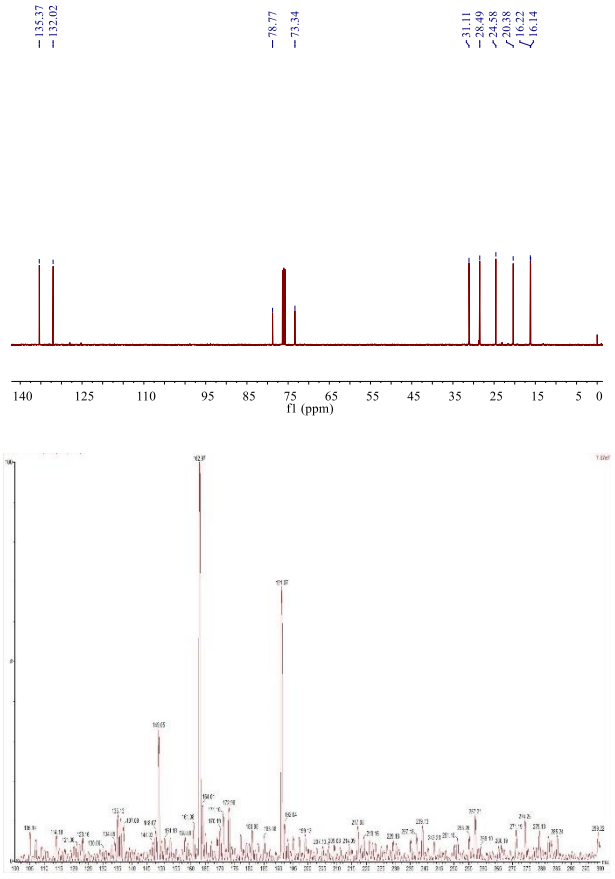

Figure 26. ^{1}H, ^{13}C, and ESI-MS spectra of the isolated photo-catalytic product ascaridole.

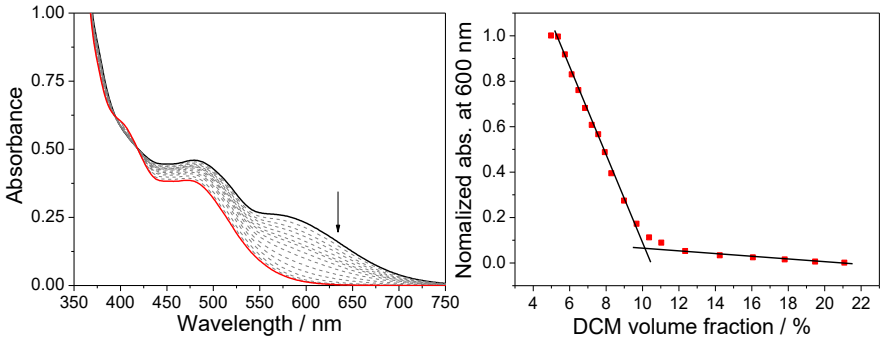

Figure S27. Solvent-dependent UV–Vis absorption spectra of **1a**/**2** in MCH/DCE (95 : 5, *v*/*v*). When "good solvent" dichloromethane (10% *v*/*v*) was added to the alternated co-assembly **1a**/**2** in MCH/DCE (95 : 5, *v*/*v*), the transition from co-assembled to molecularly-dissolved states was observed by the totally vanished MMLCT absorption signals.

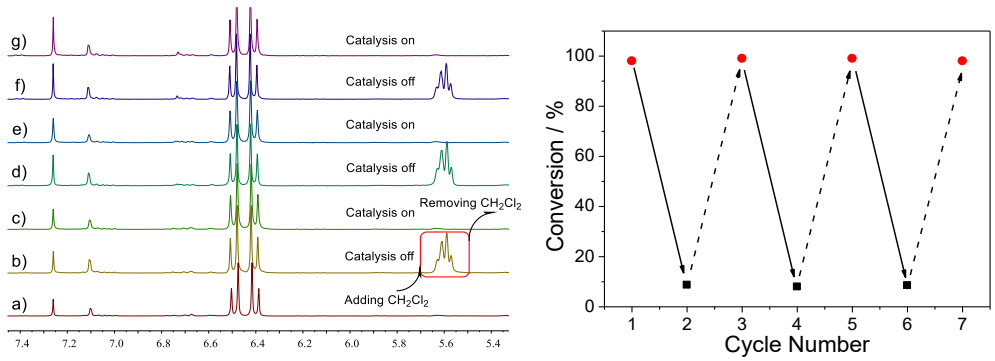

Figure S28. Monitoring photo-catalytic behaviors upon sequential addition and removal of CH_2Cl_2 (10%, *v*/*v*) into the reaction mixture (0.5% equivalence of **1a/2** when comparing to α-terpinene). Depending on the ^{1}H NMR measurements (300 MHz, $CDCl_3$, 298 K), "on-demand" photo-oxidation of *α*-terpinene can be achieved, by manipulating the reversible co-assembly of **1a**/**2**.

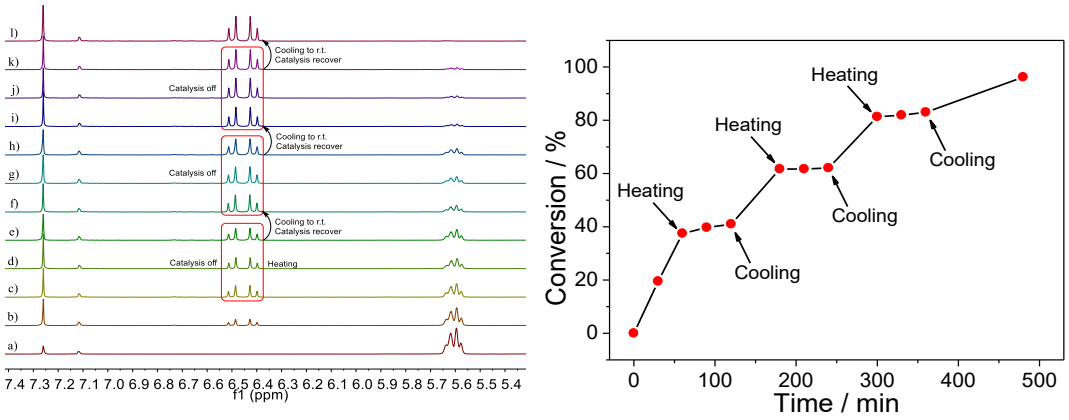

Figure S29. Monitoring photo-catalytic behaviors upon vary the temperature between 55 ºC and 25 ºC of the reaction mixture (0.5% equivalence of **1a/2** when comparing to *α*-terpinene). Depending on the ^{1}H NMR measurements (300 MHz, $CDCl_3$, 298 K), "on-demand" photo-catalytic behaviors can also be achieved by varying the temperature.

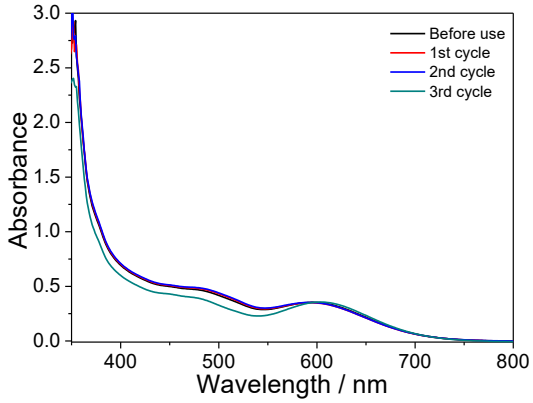

Figure 30. UV–Vis spectra of **1a/2** (0.5 mM) and *α*-terpinene (100 mM) in MCH/DCE (95 : 5, *v*/*v*) before (black line), and after three reversible photo-catalysis measurements. Particularly, the MMLCT band of copolymer **1a**/**2** at 600 nm sparingly changes after three

cycles of the stimuli-responsive photo-catalytic reaction, indicating that photo-catalytic performance still maintains.

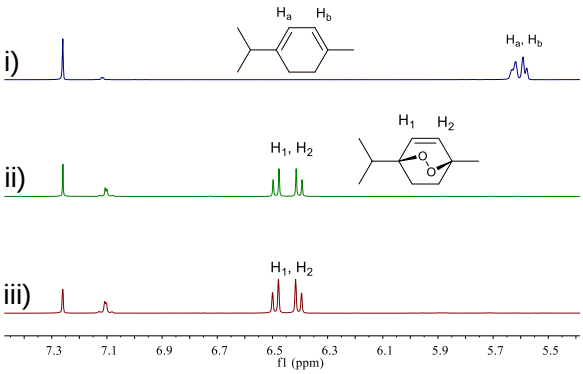

Figure 31. Partial ^{1}H NMR ($CDCl_3$, 298 K) of α-terpinene i) before, and after irradiation with 460 nm light for 12 hours by adding ii) **1a**/**2**, and iii) **1a** as the photocatalyst, respectively.

*9. Synthetic routes to monomers **1a**–**b** and **2***

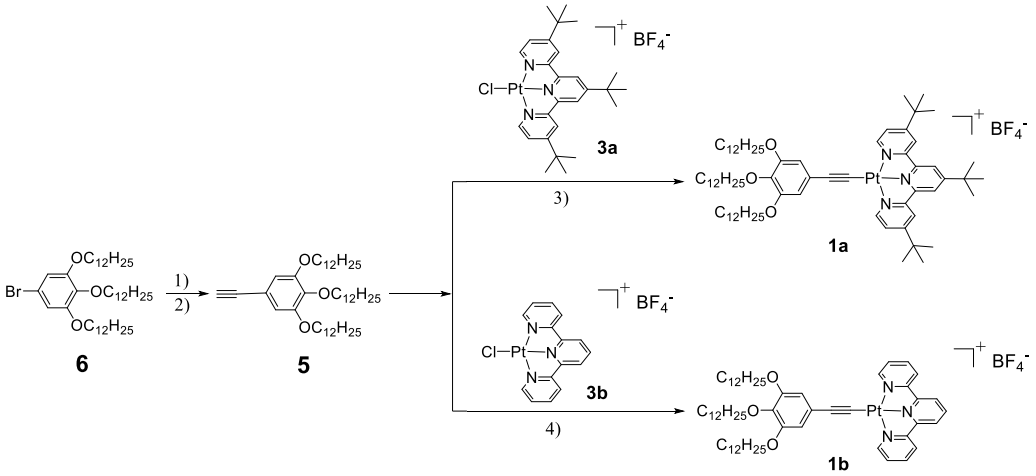

Scheme S1. Synthetic routes to monomers **1a**–**b**. 1) trimethylsilylacetylene, $Pd(PPh_3)_2Cl_2$, CuI, TEA, 55 ºC, 12 h; 2) K_2CO_3 ,CH_3OH/THF, r.t., 12 h; 3) CuI, TEA, CH_2Cl_2, r.t., 12 h; 4) CuI, TEA, DMF/CH_2Cl_2 (1 : 1, *v*/*v*), r.t., 12 h.

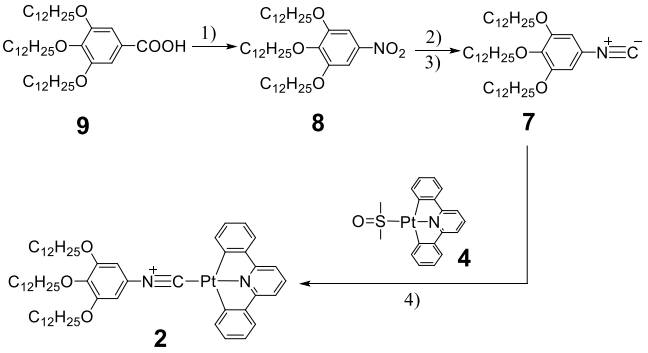

Scheme S2. Synthetic route to monomer **2**. 1) HNO_3, AIBN, MeCN, 50 ºC, 24 h; 2) N_2H_4, Pd/C, EtOH, reflux, 24 h; 3) CH_2Cl_2, $CHCl_3$, NaOH, H_2O, TEBAC, 50 ºC, 12 h; 4) CH_2Cl_2, r.t., 12 h.

*9.1. Synthesis of compound **5***

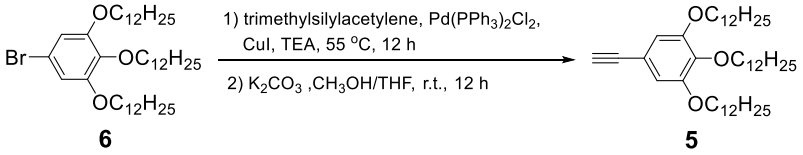

Compound **6** (1.00 g, 1.41 mmol), $Pd(PPh_3)_2Cl_2$ (50.0 mg, 0.07 mmol) and CuI (26.0 mg, 0.13 mmol) were mixed in 25 mL of TEA and stirred under nitrogen atmosphere. Trimethylsilylacetylene (554 mg, 5.64 mmol) was added dropwise to the reaction mixture over 30 minutes. After stirring at 50 ºC for 12 hours, the reaction

mixture was evaporated to remove the solvent, and the residue was purified by flash column chromatography (petroleum ether/CH_2Cl_2, 10 : 1 *v*/*v* as the eluent) to afford the product as a yellow solid (718 mg, 70 %). It was then treated with K_2CO_3 (778 mg, 5.64 mmol) in 20 mL of methanol/THF (1: 1 *v*/*v*) for 12 hours. After the deprotection reaction, the solvent was removed *in vacuo*, and the residue was extracted with H_2O/CH_2Cl_2. The combined organic extracts were dried over anhydrous Na_2SO_4 and evaporated with a rotary evaporator. The residue was purified by flash column chromatography (petroleum ether/CH_2Cl_2, 10: 1 *v*/*v* as the eluent) to afford compound **5** as a white solid (568 mg, 90%).[S10] ^{1}H NMR (300 MHz, $CDCl_3$, room temperature) δ (ppm): 6.69 (s, 2 H), 3.94 (t, 6H, J = 6.5 Hz), 2.99 (s, 1 H), 1.82–1.69 (m, 6H), 1.48–1.21 (m, 54H), 0.88 (t, 9H, J = 6.1 Hz).

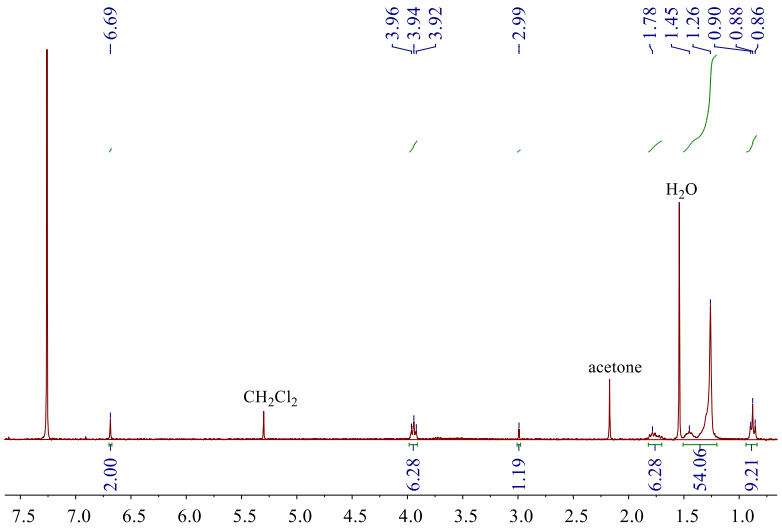

Figure S32. ^{1}H NMR spectrum (300 MHz, $CDCl_3$, room temperature) of compound **5**.

*9.2. Synthesis of monomer **1b***

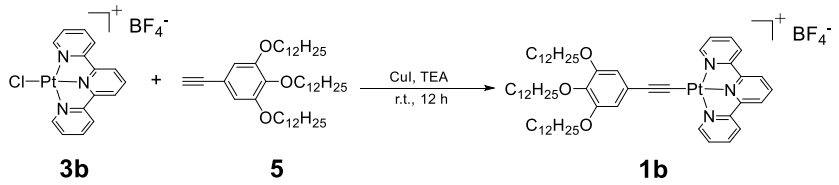

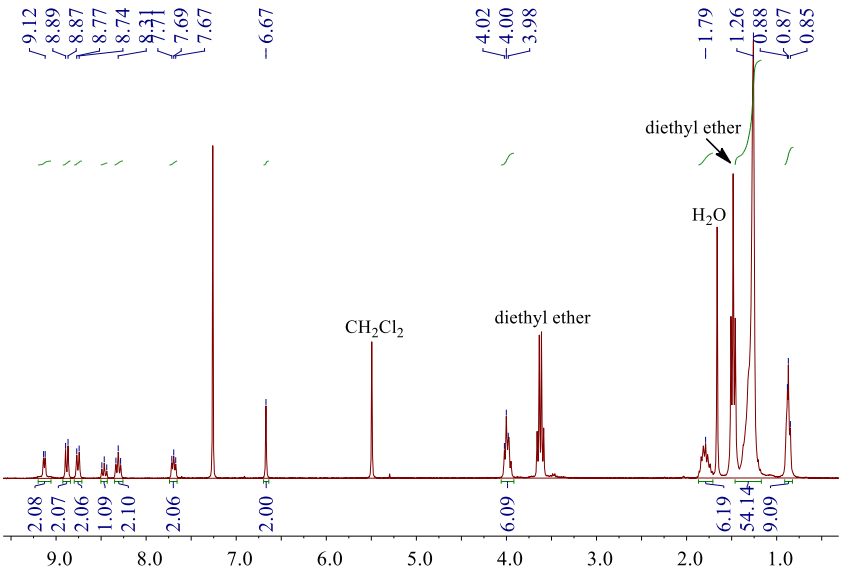

Figure S33. ^{1}H NMR spectrum (300 MHz, $CDCl_3$, room temperature) of monomer **1b**.

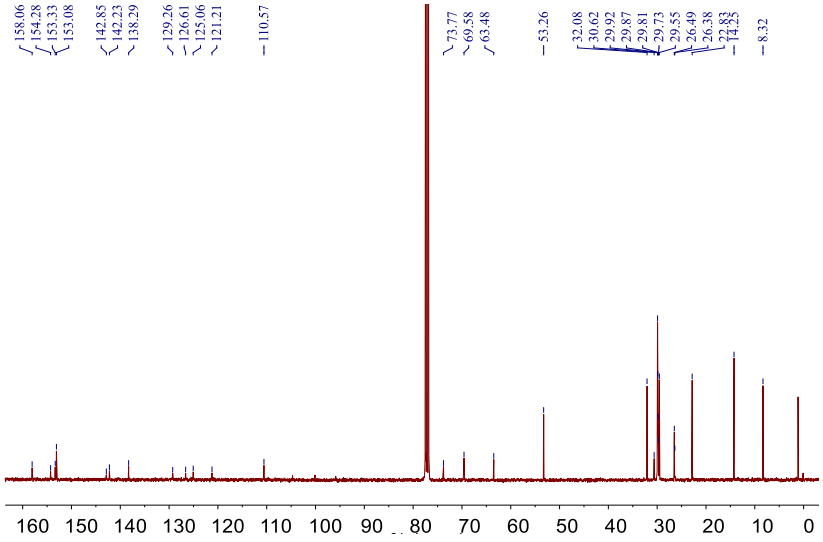

Figure S34. ^{13}C NMR spectrum (75 MHz, $CDCl_3$, room temperature) of monomer **1b**.

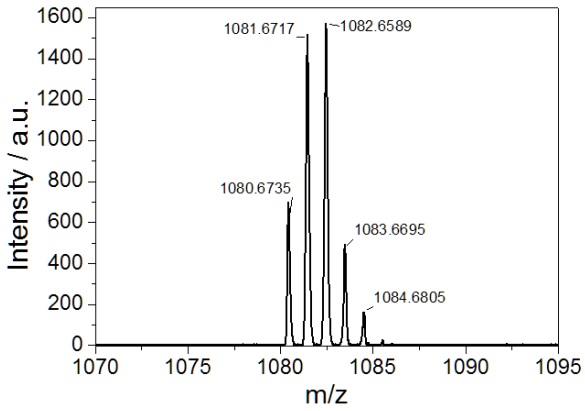

Figure S35. MALDI-TOF mass spectrum of monomer **1b**.

*9.3. Synthesis of monomer **1a***

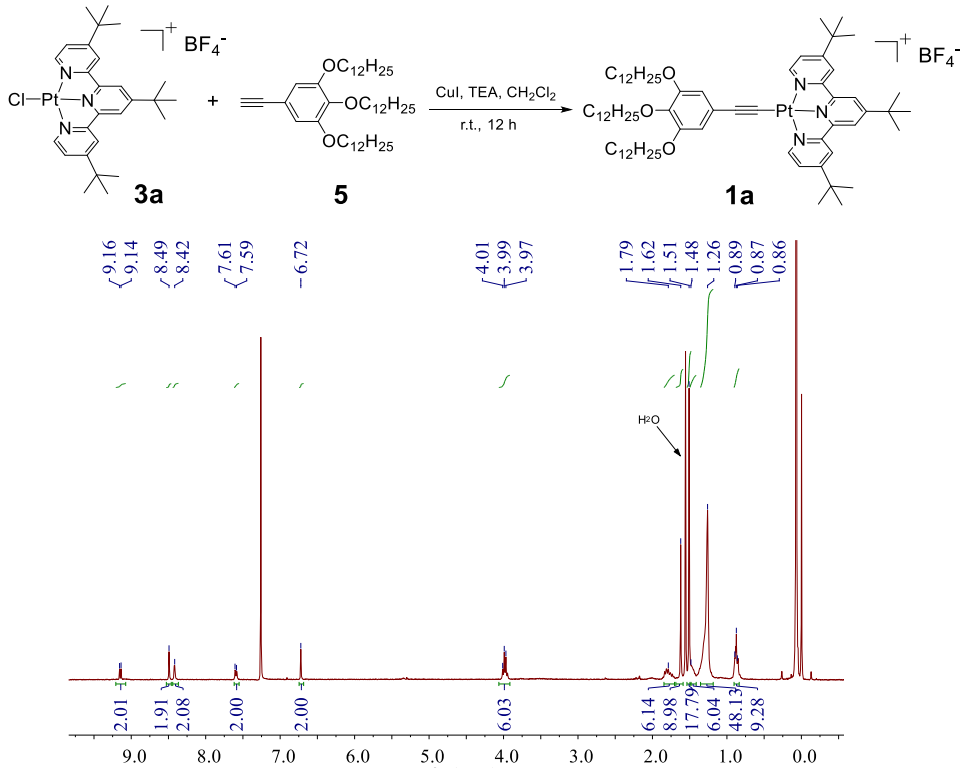

Figure S36. ^{1}H NMR spectrum (300 MHz, $CDCl_3$, room temperature) of monomer **1a**.

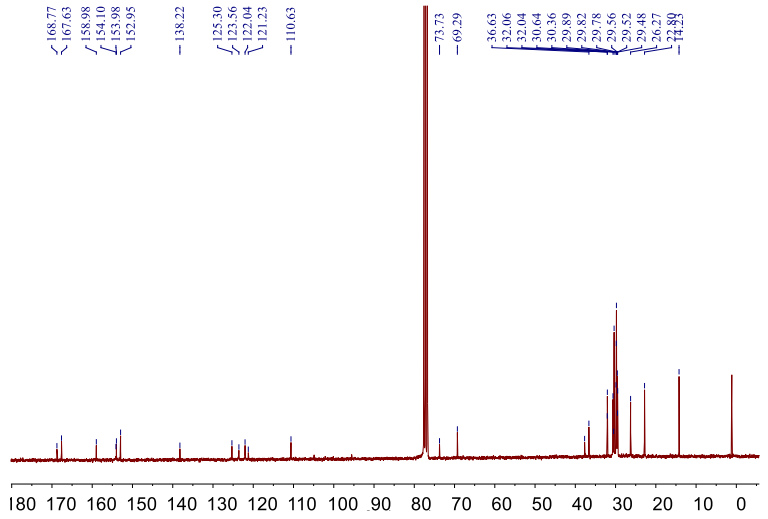

Figure S37. ^{13}C NMR spectrum (75 MHz, $CDCl_3$, room temperature) of monomer **1a**.

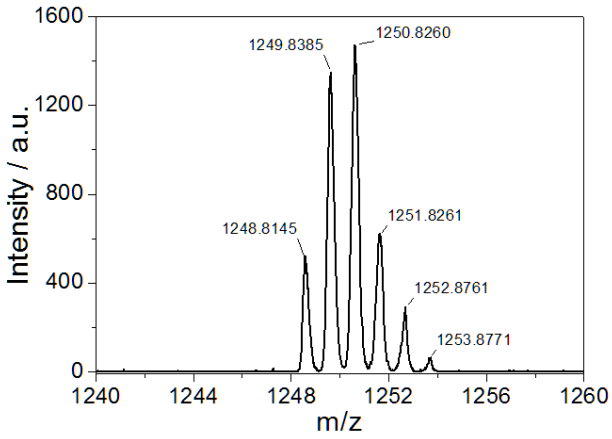

Figure S38. MALDI-TOF mass spectrum of monomer **1a**.

9.4. Synthesis of compound 7

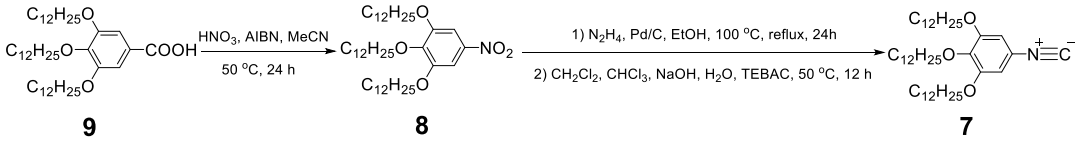

9 **8** **7**

Compound **9** (2.00 g, 2.96 mmol), nitric acid (16 M, 0.60 mL, 8.89 mmol) and AIBN (10.0 mg, 0.06 mmol) were mixed in 25 mL of MeCN, and stirred at 50 ºC for 24 hours. After the reaction was complete, ice-cold water (10 mL) was added. The organic solvent was evaporated under reduced pressure, and the residue was extracted with H_2O/CH_2Cl_2. The combined organic extracts were dried over anhydrous Na_2SO_4, and evaporated with a rotary evaporator. The residue was purified by flash column chromatography (petroleum ether/CH_2Cl_2, 3: 1 *v*/*v* as the eluent) to afford compound **8** as a pale yellow solid (1.40 g, 70%). ^{1}H NMR (300 MHz, $CDCl_3$, room temperature) δ (ppm):7.47 (s, 2H), 4.03 (t, 6H, J = 7.3 Hz), 1.88–1.79 (m, 4H), 1.77–1.69 (m, 2H), 1.53–1.45 (m, 6H), 1.40–1.19 (m, 48H), 0.88 (t, 9H, J = 6.6 Hz).

Compound **8** (500 mg, 0.74 mmol), Pd/C (30.0 mg) and N_2H_4 (85%, 3.10 mL) were added into 20 mL of EtOH, and stirred at 100 ºC for 24 hours. After the reaction was complete, the solvent was evaporated under reduced pressure, and the residue was extracted with H_2O/CH_2Cl_2. The combined organic extracts were dried over anhydrous Na_2SO_4 and evaporated with a rotary evaporator. The residue was purified by flash column chromatography (petroleum ether/CH_2Cl_2, 1: 3 *v*/*v* as the eluent) to afford 3,4,5-

tris-(dodecyloxy)aniline as a yellow solid (430 mg, 90%). It was then added to a mixture of CH_2Cl_2 (15 mL), $CHCl_3$ (8 mL), sodium hydroxide (2.00 g, 2.48 mmol), deionized water (8 mL) and benzyl triethylammonium chloride (TEBAC) (10 mg, 0.04 mmol). The reaction mixture was heated to 50 °C for 12 hours. After cooling to room temperature, the mixture was extracted with H_2O/CH_2Cl_2. The combined organic extracts were dried over anhydrous Na_2SO_4 and evaporated with a rotary evaporator. The residue was purified by flash column chromatography (petroleum ether/CH_2Cl_2, 3: 1 *v*/*v* as the eluent) to afford compound **7** as a pale yellow solid (285 mg, 70%).[S11] ^{1}H NMR (300 MHz, $CDCl_3$, room temperature) δ (ppm): 6.56 (s, 2 H),3.93 (t, 6H, J = 6.5 Hz), 1.83–1.76 (m, 4H), 1.73–1.68 (m, 2H), 1.49–1.42 (m, 6H), 1.30–1.20 (m, 48H), 0.88 (t, 9H, J = 6.8 Hz).

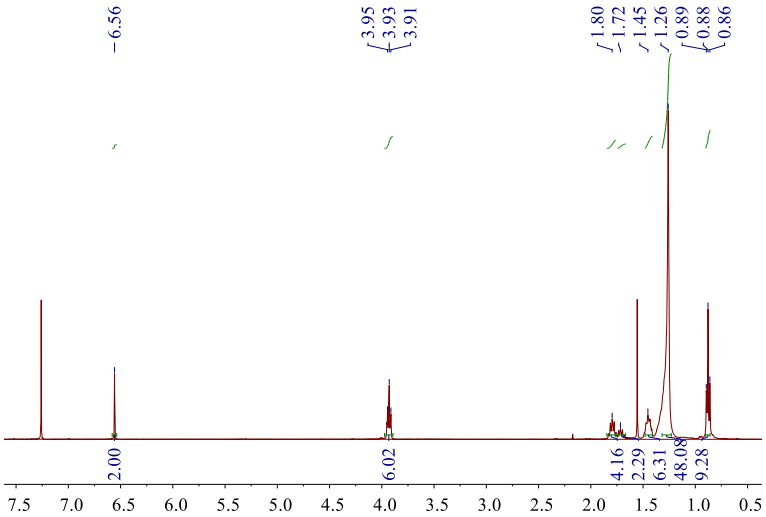

Figure S39. ^{1}H NMR spectrum (300 MHz, $CDCl_3$, room temperature) of compound **7**.

*9.5. Synthesis of monomer **2***

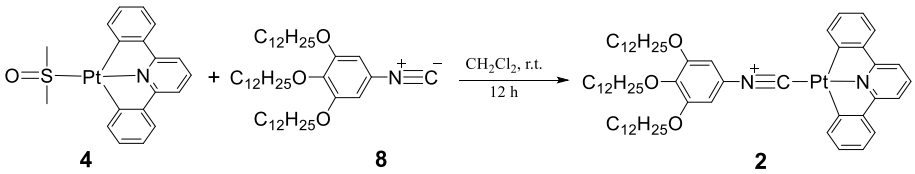

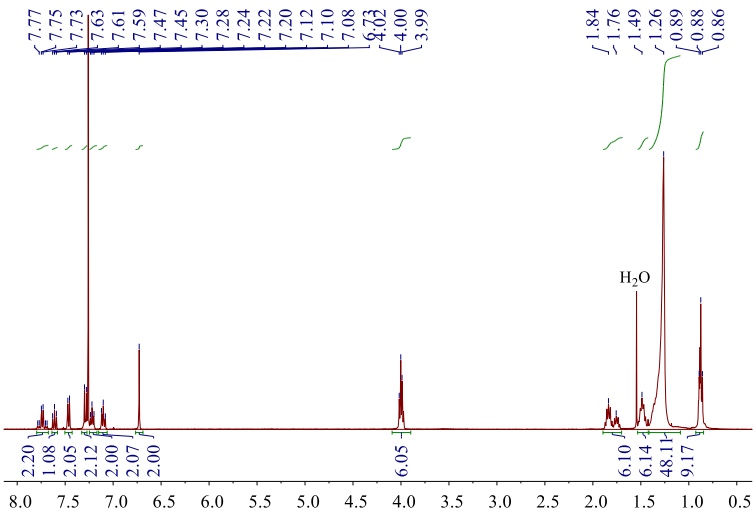

Figure S40. ^{1}H NMR spectrum (300 MHz, $CDCl_3$, room temperature) of **2**.

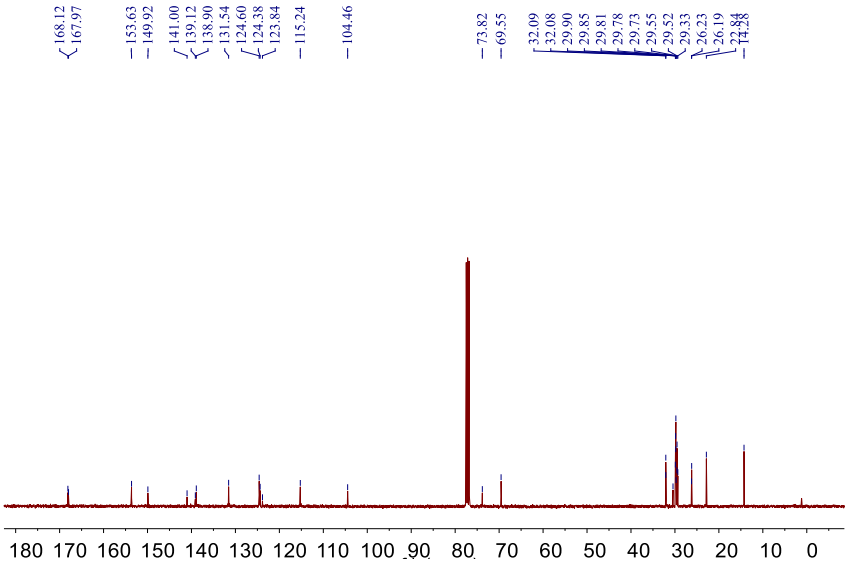

Figure S41. ^{13}C NMR spectrum (75 MHz, $CDCl_3$, room temperature) of **2**.

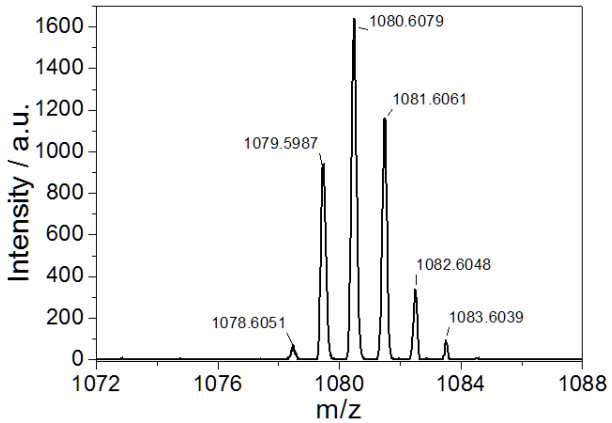

Figure S42. MALDI-TOF mass spectrum of **2**.

References:

S1. Y.-K. Tian, Y.-G. Shi, Z.-S. Yang and Wang F. *Angew. Chem., Int. Ed.,* 2014, **53**, 6090–6094.

S2. S. E. Hobert, J. T. Carney and S. D. Cummings, *Inorg. Chim. Acta,* 2001, **318**, 89–96.

S3. Y. Tanaka, K. M.-C. Wong and V. W.-W. Yam, *Chem. Sci.,* 2012, **3**, 1185–1191.

S4. T. Yasuda, T. Shimizu, F. Liu, G. Ungar and T. Kato, *J. Am. Chem. Soc.,* 2011, **133**, 13437–13444.

S5. J. Guilleme, M. J. Mayoral, J. Calbo, J. Aragó, P. M. Viruela, E. Ortí, T. Torres and D. González-Rodríguez, *Angew. Chem., Int. Ed.,* 2015*,* **54**, 2543–2547.

S6. P. Jonkheijm, P. van der Schoot, A. P. H. J. Schenning and E. W. Meijer, *Science,* 2006, **313**, 80–83.

S7. M. M. J. Smulders, M. K. L. Nieuwenhuizen, T. F. A. de Greef, P. van der Schoot, A. P. H. J. Schenning and E. W. Meijer, *Chem. Eur. J.,* 2010, **16**, 362–367.

S8. P. A. Korevaar, C. Schaefer, T. F. A. de Greef and E. W. Meijer, *J. Am. Chem. Soc.,* 2012, **134**, 13482–13491.

S9. Z. Gao, J. Zhu, Y. Han, X. Lv, X. Zhang and Feng Wang, *Polym. Chem.* **2016**, *7*, 5763–5767.

S10. V. Percec, E. Aqad, M. Peterca, J. G. Rudick, L. Lemon, J. C. Ronda, B. B. De, P. A. Heiney and E. W. Meijer, *J. Am. Chem. Soc.,* 2006, **128**, 16365–16372.

S11. A. K.-W. Chan, K. M.-C. Wong and V. W.-W. Yam, *J. Am. Chem. Soc.,* 2015, **137**, 6920–6931.